



Research article

Numerical analysis of dropper stress under a moving load based on the uplift displacement for a high-speed railway

Caizhi Yang¹, Xinxin Shen², Like Pan^{1,*}, Liming Chen¹ and Fan He^{2,*}

¹ Standards and Metrology Research Institute, China Academy of Railway Sciences Corporation Limited, Beijing, 100015, China

² School of Science, Beijing University of Civil Engineering and Architecture, Beijing, 100044, China

* **Correspondence:** Email: plk1986@126.com, hefan@bucea.edu.cn.

Abstract: The most essential cause of the fracture of the dropper is the effect of alternating stress for a long time. Therefore, in order to ensure the safe operation of high-speed railways, the influence of moving loads on the stress of a dropper was investigated in this study. Due to a high-voltage catenary system, it is very difficult to measure the moving load. Thus, the uplift displacement measured by some software and hardware devices has been applied to the contact wire instead of the moving load. The response equation for the contact wire has been derived so as to determine the initial and boundary conditions of each dropper. Then it was combined with the equation for vibration analysis of the dropper and the stress of each dropper was calculated by using the finite-difference method based on a written MATLAB program. The results show that the dropper stress, during a certain period goes through two stages of immediate rebound and bending compression when the uplift displacement is large. After the pantograph passes, the vibration of the dropper tends to be smooth; also, dropper stress variation with time can be described by three stages: immediate rebound, vibration attenuation, and bending compression. In addition, the maximum tensile stress of dropper IV was the highest. It indicates that dropper IV was more prone to fracture than other droppers.

Keywords: catenary; moving load; dropper; stress; finite-difference method

Mathematics Subject Classification: 65Z05, 74H45, 74S20

1. Introduction

The catenary system, mainly consisting of contact wire, messenger wire and droppers, is the source of power during the operation of high-speed trains. The power required for train operation is obtained through the contact between the pantograph and contact wire. The interaction could cause the violent vibration of the contact wire. Droppers are subjected to such irregular vibration and mechanical fatigue for long periods of time, which leads to frequent breakage and seriously affects the safe operation of trains. Therefore, it is necessary to study the fatigue characteristics of droppers.

Regarding dropper fatigue, researchers have designed and developed devices that could implement fatigue testing under medium- and high-frequency vibration, even under conditions of repeated bending and vibration of the dropper [1,2]. However, these test devices could not determine the stress attributed to the vibration of the dropper. Therefore, it is very difficult to determine the stress variation in the dropper with time via experimentation. In a theoretical study on the fatigue characteristics of droppers, a catenary model was mainly established by using the finite-difference method [3], the finite-element method [4] and the mode superposition method [5]. Then, the fatigue life of the dropper was predicted and the respective influences of train speed, the external environment and the position of the dropper on its fatigue life were studied [6–8]. However, the most significant cause of dropper fracture is alternating stress on the dropper; thus, it is of great significance to study it. Unfortunately, little research has been done on the effects of dropper stress on its life. Various scholars [9,10] have applied a sinusoidal force to simulate the moving load on the contact wire and studied the influence of a moving load on the stress of the dropper.

However, the catenary system is a high-voltage system, which makes it very difficult to measure the moving load. The novel aspect of the conducted research is that we have used some software and hardware devices to determine the displacement of the connection between the dropper and the contact wire when the pantograph passes; then, we applied this displacement to the contact wire instead of the moving load. Furthermore, we investigated its influence on dropper stress in this study. In the next study, we plan to utilize the results of this study to predict the fatigue life of droppers for practical application in safety estimation.

2. Vibration analysis for the contact wire

2.1. Catenary model

To simplify the analysis, the mechanical structure of the pantograph was neglected and the pantograph was simplified to a continuous moving vertical force acting on the catenary. A pantograph-catenary system with a simple chain suspension as the catenary model has been established, as shown in Figure 1. The distance between two adjacent droppers was set as 10 m. The lengths of droppers I and V were 1.6 m [11], those of droppers II and IV were 1.295 m, and that of dropper III was 1.2547 m.

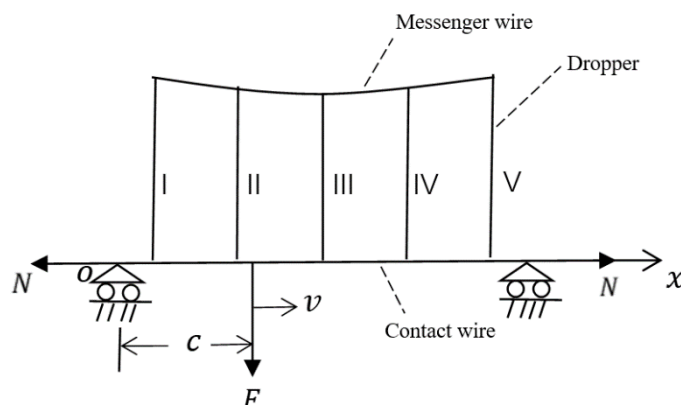


Figure 1. Mechanical model of simple chain suspension catenary.

In Figure 1, c represents the distance between the initial position of load action and the origin O . F is the contact force between the pantograph and the catenary, which varies according to time t and position x , that is to say, F could be expressed as $F(x, t)$. If the pantograph operates at a speed of v , $F(x, t)$ could be represented by the Dirac function (δ function) [12], i.e., $F(x, t) = F(t)\delta(x - (c + vt))$.

Since the catenary system is a high-voltage system, the measurement of moving load is not easy to achieve; therefore, we measured the displacement of the connection between the dropper and the contact wire by using a camera when the pantograph passes; we applied this displacement to the contact wire instead of the moving load. Therefore, $F(t)$ is expressed by the measured uplift displacement of the dropper, i.e.,

$$F(t) = K\xi(t), \quad (1)$$

where K is the stiffness of the catenary; $\xi(t)$ is the uplift displacement of the dropper. Regarding the stiffness of the catenary, the average stiffness of the catenary was applied, and its value was 3694 N/m [13]. The uplift displacement at the connection between the dropper and the contact wire was collected by hardware and software systems [14]. The hardware included a camera, rangefinder and other equipment, and the software entailed writing C++ data acquisition and data processing programs on a C++ platform. The specific process is as follows.

First, the camera was used to take pictures at equal time intervals. Then the data processing software was used to calibrate the distance-to-pixel ratio of the pictures obtained via the camera, and the corresponding relationship between the image pixels and the actual height of the structure was established. Finally, we calculated the uplift displacement at the connection between the dropper and the contact wire by calculating pixel variation as the pantograph passed.

Figure 2 shows the uplift displacement of the dropper when the high-speed train passed at 250 km/h. In Figure 3, the blue dots represent the data points extracted from Figure 2, and the green line shows the corresponding fitted curve. The function was fitted by applying Fourier analysis using a MATLAB program.

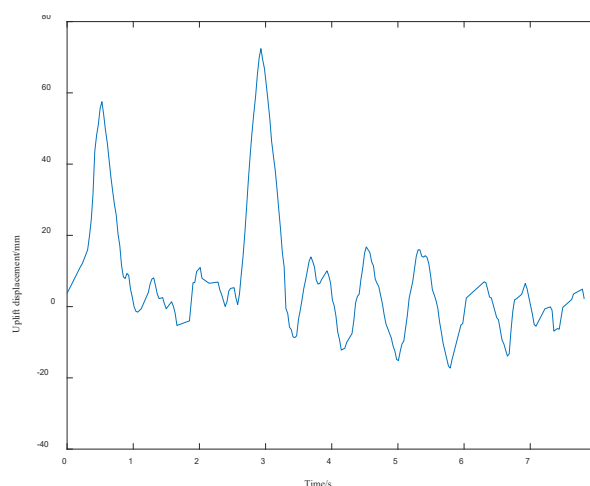


Figure 2. The uplift displacement of the dropper when the high-speed train passed at 250 km/h.

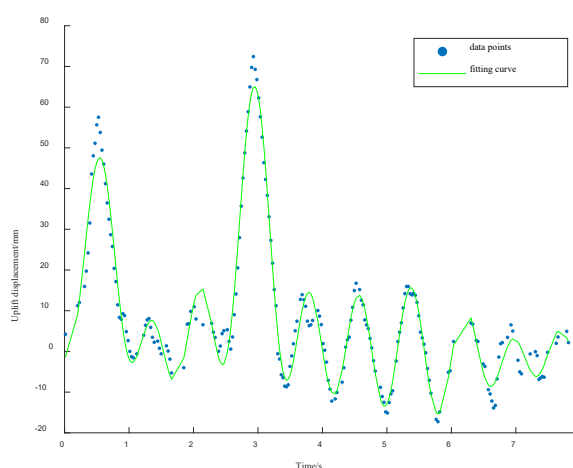


Figure 3. The result of fitting the 10th order Fourier function.

The expression of the fitting result is as follows:

$$\xi(t) = a_0 + \sum_{i=1}^N [a_i \cos(\omega_i t) + b_i \sin(\omega_i t)]$$

$$\begin{aligned} & -7.4918 - 0.4187 \cos(0.7775t) + 9.0122 \sin(0.7775t) + 2.2174 \cos(0.7775 \times 2t) \\ & -2.9705 \sin(0.7775 \times 2t) + 8.1174 \cos(0.7775 \times 3t) + 6.9552 \sin(0.7775 \times 3t) \\ & -4.2450 \cos(0.7775 \times 4t) + 7.2275 \sin(0.7775 \times 4t) + 0.2611 \cos(0.7775 \times 5t) \\ & -0.4608 \sin(0.7775 \times 5t) + 0.3921 \cos(0.7775 \times 6t) + 6.0768 \sin(0.7775 \times 6t) \\ & -7.9237 \cos(0.7775 \times 7t) + 0.6995 \sin(0.7775 \times 7t) - 0.3638 \cos(0.7775 \times 8t) \\ & -0.4300 \sin(0.7775 \times 8t) + 1.0448 \cos(0.7775 \times 9t) + 4.9803 \sin(0.7775 \times 9t) \\ & -9.8124 \cos(0.7775 \times 10t) - 7.6375 \sin(0.7775 \times 10t). \end{aligned}$$

Substituting $\xi(t)$ into Eq (1) yields $F(t)$.

2.2. Differential equation to describe contact wire motion

In order to determine the differential equation to describe contact wire motion, the contact wire was treated as a beam with equal sections. We conducted force analysis on a microscale segment of the contact wire, as shown in Figure 4.

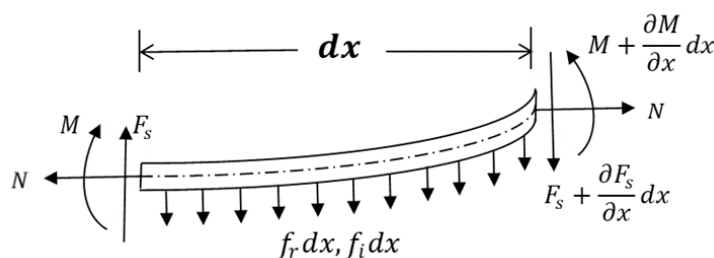


Figure 4. Force diagram for microscale segments of the contact wire that considers the tension.

In Figure4, dx is the length of the contact wire of the microscale segment, $f_r dx$ is the damping of the segment when it moves vertically, $f_i dx$ is the inertial force formed during the dynamic motion of the segment, F_s is the shear force, M is the bending moment, and N is the tension acting on both ends of the segment.

Based on D'Alembert's principle, we transformed the dynamical problem into a statics problem. The equilibrium equation in the vertical direction can be obtained as follows:

$$F_s - \left(F_s + \frac{\partial F_s}{\partial x} dx \right) - f_r dx - f_i dx = 0, \quad (2)$$

where $f_i dx$ is the inertial force of the transverse distribution of the microscale segment, which is equal to the product of the mass and acceleration of the corresponding segment, i.e.,

$$f_i dx = \rho A dx \frac{\partial^2 y(x,t)}{\partial t^2}, \quad (3)$$

where $y(x, t)$ is the transverse displacement of the contact wire, which is a binary function of the section position x and time t , ρ is the density of the contact wire, and A is the cross-sectional area of the contact wire. From Eqs (2) and (3), the equation of motion for the corresponding segment along the vertical direction could be obtained as follows:

$$\frac{\partial F_s}{\partial x} = -\rho A \frac{\partial^2 y(x,t)}{\partial t^2} - f_r. \quad (4)$$

Taking the right end of the corresponding segment as the moment center, the resultant moment of the corresponding segment is as follows:

$$M - \left(M + \frac{\partial M}{\partial x} dx \right) + N \frac{\partial y(x,t)}{\partial x} dx + F_s dx - f_r dx \frac{dx}{2} - f_i dx \frac{dx}{2} = 0. \quad (5)$$

Ignoring the higher-order trace of Eq (5), we could get

$$F_s = \frac{\partial M}{\partial x} - N \frac{\partial y(x,t)}{\partial x}. \quad (6)$$

By introducing the bending rigidity EI , the following relationship could be established from the mechanics of the materials:

$$M = EI \frac{\partial^2 y(x,t)}{\partial x^2}. \quad (7)$$

Substituting Eq (7) into Eq (6), we could get

$$F_s = \frac{\partial}{\partial x} \left[EI \frac{\partial^2 y(x,t)}{\partial x^2} \right] - N \frac{\partial y(x,t)}{\partial x}. \quad (8)$$

Substituting Eq (8) into Eq (4), we could obtain

$$\frac{\partial}{\partial x} \left[\frac{\partial}{\partial x} \left[EI \frac{\partial^2 y(x,t)}{\partial x^2} \right] - N \frac{\partial y(x,t)}{\partial x} \right] = -\rho A \frac{\partial^2 y(x,t)}{\partial t^2} - f_r, \quad (9)$$

where $f_r = C \frac{\partial y(x,t)}{\partial t}$, and C is the damping coefficient for the contact wire itself.

Thus, the equation to describe the free vibration of a beam with equal sections is as follows:

$$EI \frac{\partial^4 y(x,t)}{\partial x^4} - N \frac{\partial^2 y(x,t)}{\partial x^2} + \rho A \frac{\partial^2 y(x,t)}{\partial t^2} + C \frac{\partial y(x,t)}{\partial t} = 0. \quad (10)$$

We make the hypothesis as follows:

$$y(x, t) = Y(x)T(t). \quad (11)$$

By substituting Eq (11) into Eq (10), Eq (10) could be converted into the following equation:

$$EIY''''(x)T(t) - NY''(x)T(t) + \rho AY(x)T''(t) + CY(x)T'(t) = 0. \quad (12)$$

Separating the variables in Eq (12), we could obtain

$$\frac{EIY''''(x) - NY''(x)}{Y(x)} = -\frac{\rho AT''(t) + CT'(t)}{T(t)} = \omega, \quad (13)$$

where ω is a constant.

Multiplying $Y(x)$ to the right-hand side of the equation yields

$$EIY''''(x) - NY''(x) - \omega Y(x) = 0. \quad (14)$$

The four eigenvalues of Eq (14) can be obtained by calculation as follows:

$$\lambda_{1,2} = \pm \sqrt{\frac{N}{2EI} + \sqrt{\left(\frac{N}{2EI}\right)^2 + \frac{\omega}{EI}}} = \pm k_1,$$

$$\lambda_{3,4} = \pm i \sqrt{-\frac{N}{2EI} + \sqrt{\left(\frac{N}{2EI}\right)^2 + \frac{\omega}{EI}}} = \pm ik_2.$$

Then, the general solution of Eq (14) is given by

$$Y(x) = B_1 e^{k_1 x} + B_2 e^{-k_1 x} + B_3 e^{ik_2 x} + B_4 e^{-ik_2 x}.$$

Given the following:

$$\begin{cases} e^{\pm k_1 x} = \cosh k_1 x \pm \sinh k_1 x, \\ e^{\pm i k_2 x} = \cos k_2 x \pm i \sin k_2 x. \end{cases}$$

$Y(x)$ takes the following form:

$$Y(x) = D_1 \cosh k_1 x + D_2 \sinh k_1 x + D_3 \cos k_2 x + D_4 \sin k_2 x. \quad (15)$$

Since there are supports at both ends of the contact wire, the displacement and bending moment at both ends are equal to zero. Hence, we have the following boundary conditions:

$$\begin{cases} Y(0) = 0, \\ Y''(0) = 0, \\ Y(l) = 0, \\ Y''(l) = 0. \end{cases} \quad (16)$$

Thus, we could get

$$\begin{aligned} D_1 = D_2 = D_3 &= 0, \\ \sin k_2 l &= 0. \end{aligned}$$

Then, we have

$$k_2 = \frac{i\pi}{l} (i = 1, 2, 3, \dots).$$

The following expression can be obtained:

$$Y_i(x) = \sin \frac{i\pi}{l} x (i = 1, 2, 3, \dots). \quad (17)$$

If the pantograph travels forward at the speed v , then the forced vibration of the beam is given by

$$EI \frac{\partial^4 y(x,t)}{\partial x^4} - N \frac{\partial^2 y(x,t)}{\partial x^2} + \rho A \frac{\partial^2 y(x,t)}{\partial t^2} + C \frac{\partial y(x,t)}{\partial t} = F(t) \delta(x - (c + vt)). \quad (18)$$

Substituting Eq (1) into Eq (18) yields

$$EI \frac{\partial^4 y(x,t)}{\partial x^4} - N \frac{\partial^2 y(x,t)}{\partial x^2} + \rho A \frac{\partial^2 y(x,t)}{\partial t^2} + C \frac{\partial y(x,t)}{\partial t} = K \xi(t) \delta(x - (c + vt)). \quad (19)$$

Then, the solution of Eq (19) could be expressed as

$$y(x,t) = \sum_{i=1}^{\infty} Y_i(x) q_i(t). \quad (20)$$

Substituting Eq (20) into Eq (19), we could obtain

$$\sum_{i=1}^{\infty} [EI Y_i''''(x) q_i(t) - N Y_i''(x) q_i(t) + \rho A Y_i(x) q_i''(t) + C Y_i(x) q_i'(t)] = K \xi(t) \delta(x - (c + vt)). \quad (21)$$

Then, multiply both sides of Eq (21) by $Y_i(x)$ and integrate x along the beam length to get

$$\begin{aligned}
& EI \int_0^l \sum_{i=1}^{\infty} Y_i'''(x) Y_j(x) q_i(t) dx - N \int_0^l \sum_{i=1}^{\infty} Y_i''(x) Y_j(x) q_i(t) dx + \\
& \rho A \int_0^l \sum_{i=1}^{\infty} Y_i(x) Y_j(x) q_i''(t) dx + C \int_0^l \sum_{i=1}^{\infty} Y_i(x) Y_j(x) q_i'(t) dx \\
& = \int_0^l K \xi(t) \delta(x - (c + vt)) Y_j(x) dx
\end{aligned} \tag{22}$$

We have

$$\begin{aligned}
Y_i^{(2n)}(x) &= (-1)^n \left(\frac{i\pi}{l}\right)^{2n} Y_i(x), \\
\int_0^l Y_i(x) Y_j(x) dx &= \frac{l}{2} \quad (i = j), \\
\int_0^l Y_i(x) Y_j(x) dx &= 0 \quad (i \neq j), \\
\int_0^l \delta(x - (c + vt)) Y_j(x) dx &= Y_j(c + vt).
\end{aligned}$$

Thus, Eq (22) is transformed into the following equation:

$$\left(\frac{EIj^4\pi^4}{2l^3} + \frac{Nj^2\pi^2}{2l}\right) q_j(t) + \frac{Cl}{2} q_j'(t) + \frac{\rho Al}{2} q_j''(t) = K\xi(t) \sin \frac{j\pi(c+vt)}{l}. \tag{23}$$

Equation (23) is a second-order ordinary differential equation, which is solved numerically by applying a finite-difference method [15]. First, $[0, T]$ is divided into N equal intervals, and the divided points are obtained as follows:

$$t_i = i \cdot \Delta t, \quad i = 0, 1, \dots, N,$$

where t_i is the node; Δt is the time step.

We use q_i to represent the value of function $q(t)$ at node t_i , and then we apply a central difference scheme; it follows that

$$\begin{aligned}
\frac{d^2q}{dt^2} &= \frac{q_{i+1} - 2q_i + q_{i-1}}{\Delta t^2}, \\
\frac{dq}{dt} &= \frac{q_{i+1} - q_{i-1}}{2 \cdot \Delta t}.
\end{aligned}$$

Let

$$\begin{aligned}
a &= \frac{\rho Al}{2}, \\
b &= \frac{Cl}{2}, \\
p &= \frac{EIj^4\pi^4}{2l^3} + \frac{Nj^2\pi^2}{2l}, \\
M(t) &= K\xi(t) \sin \frac{j\pi(c + vt)}{l}.
\end{aligned}$$

Then, the finite-difference scheme of Eq (23) is given by

$$a \cdot \frac{q_{i+1} - 2q_i + q_{i-1}}{\Delta t^2} + b \cdot \frac{q_{i+1} - q_{i-1}}{2 \cdot \Delta t} + p \cdot q_i = M(t_i). \quad (24)$$

Thus, we obtain

$$\left(\frac{a}{\Delta t^2} + \frac{b}{2 \cdot \Delta t}\right) q_{i+1} + \left(p - \frac{2a}{\Delta t^2}\right) q_i + \left(\frac{a}{\Delta t^2} - \frac{b}{2 \cdot \Delta t}\right) q_{i-1} = M(t_i). \quad (25)$$

We apply the initial and boundary conditions $q(0) = q(T) = 0$.

Let

$$A = \begin{bmatrix} p - \frac{2a}{\Delta t^2} & \frac{a}{\Delta t^2} + \frac{b}{2 \cdot \Delta t} & 0 & \cdots & 0 & 0 \\ \frac{a}{\Delta t^2} - \frac{b}{2 \cdot \Delta t} & p - \frac{2a}{\Delta t^2} & \frac{a}{\Delta t^2} + \frac{b}{2 \cdot \Delta t} & \cdots & 0 & 0 \\ 0 & \frac{a}{\Delta t^2} - \frac{b}{2 \cdot \Delta t} & p - \frac{2a}{\Delta t^2} & \cdots & 0 & 0 \\ \cdots & \cdots & \cdots & \cdots & \cdots & \cdots \\ 0 & 0 & 0 & \cdots & \frac{a}{\Delta t^2} - \frac{b}{2 \cdot \Delta t} & p - \frac{2a}{\Delta t^2} \end{bmatrix},$$

$$Q = (q_1, q_2, \dots, q_{N-1})^T,$$

$$r = (M(t_1), M(t_2), \dots, M(t_{N-1}))^T.$$

Then

$$AQ = r. \quad (26)$$

Equation (26) is a tridiagonal system of equations. Therefore, the q value of each time node could be obtained by using a MATLAB program to implement the forward elimination and backward substitution.

The influence of the higher order is very small; thus, only the first five orders need to be calculated. Therefore, the response equation for the contact wire is given by

$$y(x, t) = \sum_{j=1}^5 Y_j(x) q_j(t). \quad (27)$$

3. Calculation of dropper stress

3.1. Vibration analysis for the dropper

In order to study the stress variation of a dropper in the process of vibration, the force analysis of its microscale segment was carried out, as shown in Figure 5.

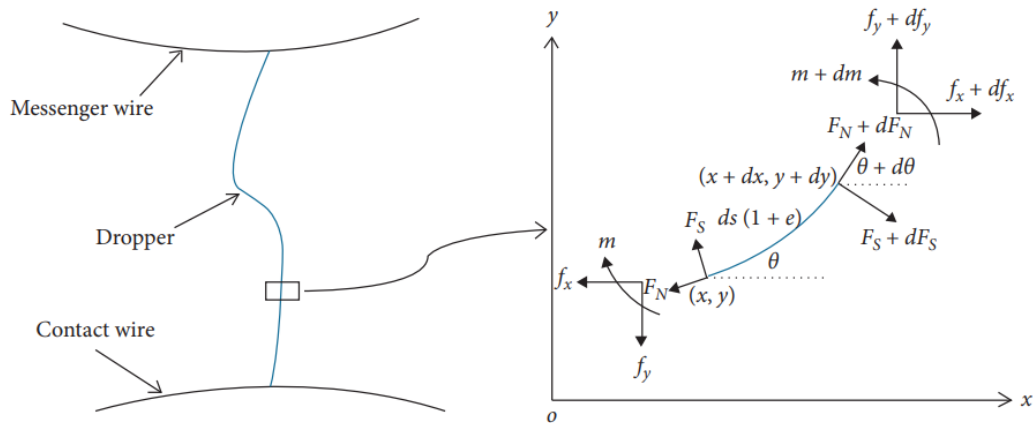


Figure 5. Force analysis diagram for the dropper.

In Figure 5, f_x and f_y are the forces applied on the corresponding segment along the horizontal direction and the vertical direction, respectively. m is the bending moment, F_N is the axial tension, F_S is the shear force, θ is the angle between the corresponding segment and the horizontal direction.

To simplify the calculation, we can introduce dimensionless variables:

$$\bar{x} = \frac{x}{L}, \bar{y} = \frac{y}{L}, \bar{s} = \frac{s}{L}, \bar{v}_x = \frac{v_x}{\sqrt{gL}}, \bar{v}_y = \frac{v_y}{\sqrt{gL}}, \bar{f}_x = \frac{f_x}{E_d A_d}, \bar{f}_y = \frac{f_y}{E_d A_d},$$

$$\bar{m} = \frac{m}{E_d A_d L}, \bar{t} = \frac{t}{\sqrt{L/g}}, \mu = \frac{\rho_d g L}{E_d}, \lambda^2 = \frac{E_d A_d L^2}{E_d I_d}, \bar{c}_d = \frac{c_d \sqrt{gL}}{E_d A_d},$$

where x and y are the position coordinates, s is the arc coordinate, L represents the total length of the dropper, v_x and v_y are the velocities of motion in the x direction and the y direction, respectively, g is the acceleration of gravity, E_d is the elastic modulus of the dropper, A_d is the cross-sectional area of the dropper, t is time, ρ_d is the density of the dropper, $E_d I_d$ is the bending stiffness of the dropper, and c_d is the dropper damping coefficient.

Thus, the following equations could be obtained via force analysis.

$$\begin{cases} \sqrt{\left(\frac{\partial \bar{x}}{\partial \bar{s}}\right)^2 + \left(\frac{\partial \bar{y}}{\partial \bar{s}}\right)^2} - 1 = \bar{f}_x \cos \theta + \bar{f}_y \sin \theta, \\ \frac{\partial \bar{m}}{\partial \bar{s}} = \bar{f}_x \sin \theta - \bar{f}_y \cos \theta, \\ \frac{\partial \theta}{\partial \bar{s}} = \lambda^2 \bar{m}, \\ \frac{\partial \bar{f}_x}{\partial \bar{s}} - \bar{c}_d \bar{v}_x = \mu \frac{\partial^2 \bar{x}}{\partial \bar{t}^2}, \\ \frac{\partial \bar{f}_y}{\partial \bar{s}} - \bar{c}_d \bar{v}_y = \mu \frac{\partial^2 \bar{y}}{\partial \bar{t}^2} + \mu, \\ \frac{d\bar{y}}{d\bar{x}} = \tan \theta. \end{cases} \quad (28)$$

The stress of the dropper can be calculated based on the above equation.

$$\sigma = \frac{F_N}{A_d} + \frac{m}{w_z}, \quad (29)$$

where $F_N = f_x \cos\theta + f_y \sin\theta$ and w_z is the section modulus in bending of the dropper.

3.2. Initial and boundary conditions of each dropper

The initial condition of a dropper is the case that $t = 0$, which means that the dropper is not subjected to any external force and is in a natural straightened state. The x positions of the five droppers were 5, 15, 25, 35, and 45, respectively, which could be uniformly expressed as follows: $5 + 10(i - 1)$, $i = 1, 2, 3, 4, 5$. The y position was set as the arc coordinate of the corresponding segment of the dropper.

The boundary conditions for dropper were applied as the conditions at the connection point between the dropper and the contact wire and the conditions at the connection point between the dropper and the messenger wire. In the case of the connection point between the dropper and the contact wire, the x positions were still 5, 15, 25, 35, and 45, respectively. The y position corresponded to the response of the contact wire at the x position of the dropper ($x=5, 15, 25, 35, 45$). The vibrational response of the messenger wire was not considered in this study. Assuming that the arc coordinate at the connection point between the dropper and the contact wire was 0, we set the arc coordinate at the connection point between the dropper and the messenger wire to be L_i ($i = 1, 2, 3, 4, 5$).

For droppers at different positions, their initial and boundary conditions are different. However, the initial and boundary conditions of each dropper after introducing dimensionless variables could be uniformly expressed in the following form:

$$\begin{cases} \bar{x}(\bar{s}, \bar{t}) = \frac{5 + 10(i - 1)}{L_i} \\ \bar{y}(\bar{s}, \bar{t}) = \bar{s} \end{cases}, \text{ when } \bar{t} = 0,$$

$$\begin{cases} \bar{x}(\bar{s}, \bar{t}) = \frac{5 + 10(i - 1)}{L_i} \\ \bar{y}(\bar{s}, \bar{t}) = \left(\sum_{j=1}^5 Y_j(x) q_j(t) \right) / L_i \end{cases}, \text{ when } \bar{s} = 0,$$

$$\begin{cases} \bar{x}(\bar{s}, \bar{t}) = \frac{5 + 10(i - 1)}{L_i} \\ \bar{y}(\bar{s}, \bar{t}) \leq 1 \end{cases}, \text{ when } \bar{s} = 1,$$

where i is the number of the dropper, L_i is the length of each dropper, \bar{s} is the dimensionless arc coordinate, \bar{t} is dimensionless time, \bar{x} and \bar{y} are dimensionless position coordinates, $\sum_{j=1}^5 Y_j(x) q_j(t)$ is the response of the contact wire as described in Section 2.2.

3.3. Parameters for the dropper and contact wire

The elastic moduli of the dropper and the contact wire were measured by using a universal testing machine and electronic extensometer, and the bending stiffness was calculated based on the

Costello model [16]. When calculating the stress on a dropper, the specific values of the dropper and contact wire parameters were as shown in Tables 1 and 2, respectively.

Table 1. Parameters for the dropper.

Density ($kg \cdot m^{-3}$)	Cross-sectional area (m^2)	Elastic modulus (Pa)	Bending stiffness ($Pa \cdot m^4$)	Section modulus in bending (m^3)	Damping coefficient
8.9×10^3	1.29×10^{-5}	83.29×10^9	2.53	6.7663×10^{-9}	10

Table 2. Parameters for the contact wire.

Density ($kg \cdot m^{-3}$)	Cross-sectional area (m^2)	Elastic modulus (Pa)	Bending stiffness ($Pa \cdot m^4$)	Tension (N)	Damping coefficient
8.9×10^3	1.58×10^{-4}	118.49×10^9	233.92	3×10^4	1

3.4. Numerical method

Equation (28) is a group of partial differential equations, and it is difficult to obtain its analytical solution. Therefore, the finite-difference method was used to obtain the numerical solution in this study; the specific steps are as follows.

(1) The dropper was discretized into n units of equal length. The number of discrete elements and the selection of time step affect the accuracy of the numerical solution. The larger the number of discrete elements and the smaller the time step, the higher the accuracy of the numerical solution; however, the computational time also increases. For the 1.6-m-length droppers I and V, we selected the number of discrete elements (4, 8, 16, 32, 64, 128) for the trial calculation. We found that the calculated results did not converge when n was less than or equal to 16. When n was 32, the calculated results were not much different from those obtained for $n=64$ and 128; also, the resulting values of the dropper force from these elements were found to agree to within 4%. However, when n was 64 or 128, the computational time was very long. Therefore, the value of n in this study was set to 32, and the dimensionless time step was 7.5×10^{-8} .

(2) We selected the finite-difference scheme. The partial differential with respect to the arc coordinate and time in the equations could be expressed approximately as follows:

$$\frac{\partial \bar{x}}{\partial \bar{s}} = \frac{\bar{x}_{i+1} - \bar{x}_i}{\Delta \bar{s}},$$

$$\frac{\partial \bar{y}}{\partial \bar{s}} = \frac{\bar{y}_{i+1} - \bar{y}_i}{\Delta \bar{s}},$$

$$\frac{\partial \bar{m}}{\partial \bar{s}} = \frac{\bar{m}_{i+1} - \bar{m}_i}{\Delta \bar{s}},$$

$$\frac{\partial \theta}{\partial \bar{s}} = \frac{\theta_{i+1} - \theta_i}{\Delta \bar{s}},$$

$$\frac{\partial \bar{f}_x}{\partial \bar{s}} = \frac{\bar{f}_{x_{i+1}} - \bar{f}_{x_i}}{\Delta \bar{s}},$$

$$\frac{\partial \bar{f}_y}{\partial \bar{s}} = \frac{\bar{f}_{y_{i+1}} - \bar{f}_{y_i}}{\Delta \bar{s}},$$

$$\frac{d\bar{y}}{d\bar{x}} = \frac{\bar{y}_{i+1} - \bar{y}_i}{\bar{x}_{i+1} - \bar{x}_i},$$

$$\frac{\partial^2 \bar{x}}{\partial \bar{t}^2} = \frac{\bar{x}_{i+2} - 2\bar{x}_{i+1} + \bar{x}_i}{\Delta \bar{t}^2},$$

$$\frac{\partial^2 \bar{y}}{\partial \bar{t}^2} = \frac{\bar{y}_{i+2} - 2\bar{y}_{i+1} + \bar{y}_i}{\Delta \bar{t}^2}.$$

(3) Substituting the above expressions into the equations, the difference equations to describe dropper vibration could be obtained.

(4) Combining the initial and boundary conditions, the stress variation diagram for the dropper could be obtained by writing a MATLAB program.

4. Results

When the high-speed train runs from left to right starting from the third dropper at a speed of 250 km/h, the stress variation of dropper I is as shown in Figure 6.

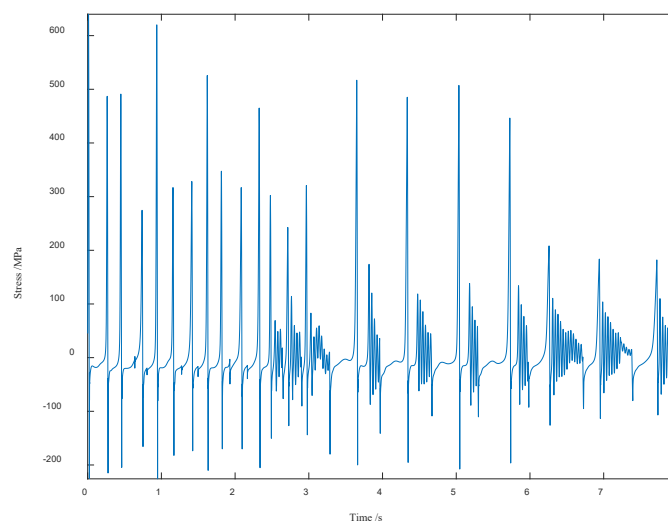


Figure 6. The stress variation for dropper I with time.

The moving load acting on the contact wire will cause vibration of the contact wire, and the dropper will also vibrate under the influence of the contact wire; consequently, the stress of the dropper

will change. It can be seen that the vibration of the dropper has obvious periodicity, and that the stress fluctuates quickly. In the first 2 seconds, a period of dropper stress goes through the two stages of immediate rebound and bending compression, and there is almost no attenuated vibration stage. In the last 5 seconds, one period of stress variation goes through three stages: immediate rebound, vibration attenuation, and bending compression, and the attenuation time gradually becomes longer.

The stress variation of dropper II is shown in Figure 7. It can be seen that the stress variation of dropper II was different from that of dropper I. The biggest difference is that the maximum tensile stress of dropper II was higher than that of dropper I.

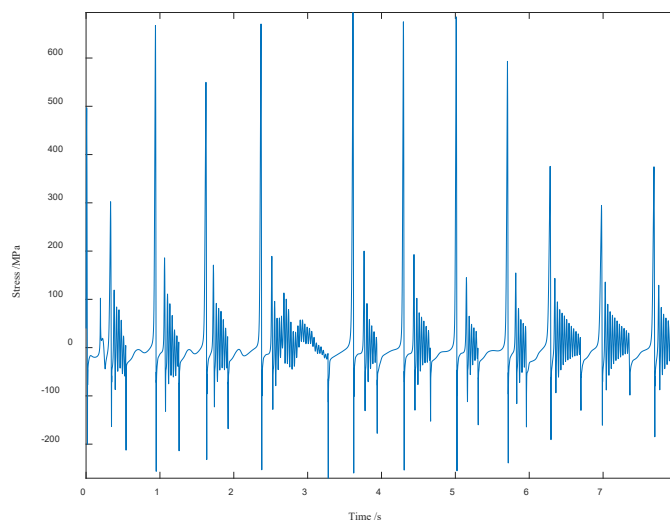


Figure 7. The stress variation for dropper II with time.

According to Figure 8, the stress fluctuates quickly, which is the same as that for droppers I and II. The difference is the length of time to reach the maximum tensile and compressive stresses. In addition, the degree of vibration of dropper III was more intense than that of droppers I and II.

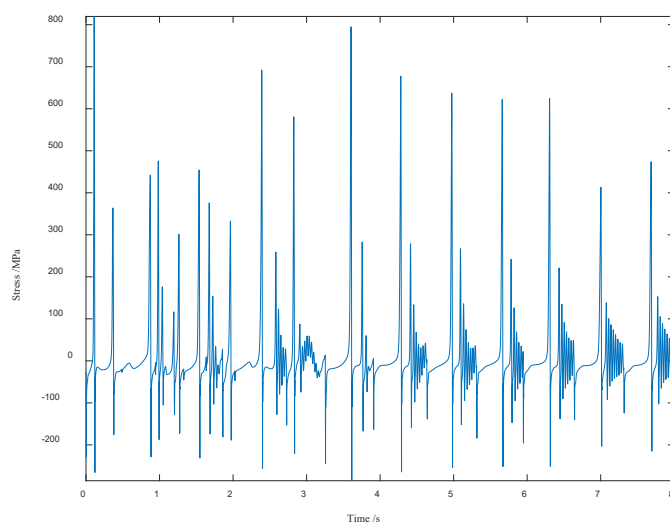


Figure 8. The stress variation for dropper III with time.

The stress variation of dropper IV is shown in Figure 9. It is obvious that the maximum tensile stress value for dropper IV was higher than that for droppers I, II and III.

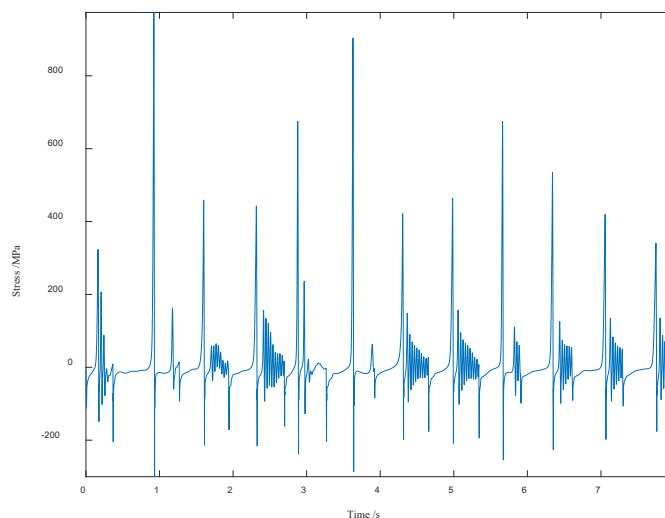


Figure 9. The stress variation for dropper IV with time.

The stress variation of dropper V was the same as that of dropper I, as shown in Figure 10. They all went through the two stages of immediate rebound and bending compression in the earlier time, and then the three stages of immediate rebound, vibration attenuation, and bending compression in the later time. However, due to the different positions in the catenary, the maximum tensile and compressive stress values for droppers V and I were different.

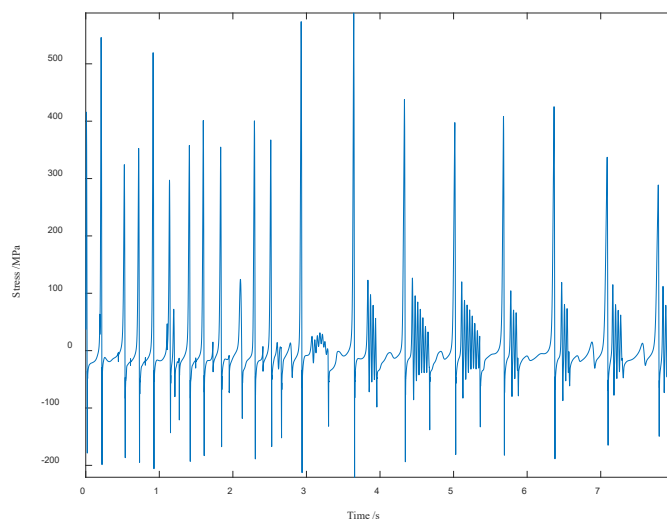


Figure 10. The stress variation for dropper V with time.

5. Discussion

Because the dropper in the straightened state suffers significantly under the action of loading, the lifting force makes the dropper change to a relaxed state; then, the dropper returns to the stretched state because of gravity. Therefore, in a period, dropper stress variation with time can be categorized as having three stages, i.e., immediate rebound, vibration attenuation, and bending compression, but not all periods go through three stages. The moving load acting on the contact wire causes vibration of the contact wire, and this vibration propagates to the left and right in the form of waves. Therefore, no matter where the moving load acts on the contact wire, all of the droppers in the catenary will vibrate; the dropper stress will also change with the vibration. When the moving load acts on a certain point of the contact wire, the amplitude of the dropper decreases as the distance between the dropper and the position where the load acts becomes farther; this is due to the energy loss of the wave during its propagation. However, because the moving load continues to act on the contact wire, the maximum tensile and compressive stress values for dropper IV were found to be higher than those for dropper III.

The catenary structure is symmetric, but because the moving load moves from left to right at a certain speed, the stress variations of five droppers are not symmetric across the catenary. By observing the stress variation of each dropper, it was found that the stress variations of the droppers in different positions are different. Therefore, the influence of the position of the dropper on the stress should not be ignored. It was also found that the maximum tensile stress of dropper IV was higher than that of the other droppers, indicating that dropper IV is more likely to fracture than other droppers, which is consistent with the statistical results of Yu et al. [17]. Thus, the model in this paper is validated.

When the train passes, there is an interaction between the contact wire and the dropper, but the force of the dropper on the contact wire was not considered when the force analysis was performed on the microscale segment of the contact wire in this study. In order to make the model more realistic, the force of the dropper on the contact wire should be taken into account in future studies.

Exploring dynamic loading conditions that more accurately mirror real-life stressors on the railway system and incorporating the wear and degradation over time into the analysis could provide a more comprehensive understanding of dropper longevity. Further studies might also explore the impact of different parameters on dropper stress, the frequency of dropper vibration, and the potential for resonance-induced failures. Expanding the analysis to three dimensions could yield insights into the complex stress patterns that emerge under varied conditions. Probabilistic methods could be employed to gauge failure likelihood, thereby informing maintenance schedules and promoting the safe operation of high-speed railways. In addition, the influence of corrosion on dropper fatigue life should not be overlooked. Finally, integrating multiscale modeling could link material behavior at the micro-level with overall structural performance, offering a richer, more nuanced view of dropper stresses. It should be noted that risk analysis deals with inherent uncertainties that mainly arise from system complexity, insufficient data, and the applied risk model's associated assumptions and incapability. The digitalized process systems can be monitored and maintained with the greatest efficiency and control among all existing process safety domains. Thus, it leads to overconfidence in instrumentation and data utilization, which adversely affects process safety [18]. In the future work, the integration of uncertainty modeling into our analysis would not only enhance the current study, it would also pave the way for future research to build upon a more solid and quantitatively assessed foundation.

6. Conclusions

In this paper, the uplift displacement of droppers was applied to the contact wire instead of the moving load, and the influence on dropper stress was studied. The conclusions could be drawn as follows.

- (1) The variation in dropper stress with time generally goes through three stages: Immediate rebound, vibration attenuation, and bending compression. However, when the uplift displacement of a dropper suddenly increases and the dropper is greatly impacted, there is almost no vibration attenuation stage in the vibration process and there is a large bending deformation.
- (2) The variation of dropper stress is different for different positions; thus, the influence of the position of the dropper on the stress should not be ignored.
- (3) The maximum tensile stress value for dropper IV was found to be higher than that for other droppers, indicating that dropper IV is more prone to fracture than other droppers.

Use of AI tools declaration

The authors declare that they have not used Artificial Intelligence tools in the creation of this article.

Acknowledgments

This work was supported by the Research Project of China Academy of Railway Sciences Corporation Limited(2022YJ168).

Conflict of interest

The authors declare that they have no conflicts of interest.

References

1. J. Ruan, H. B. Yuan, H. M. Li, H. Y. Xu, Design and application of vibratory fatigue test rig for high speed railway OCS dropper, *China Railway*, **2020** (2020), 117–122. <https://doi.org/10.19549/j.issn.1001-683x.2020.08.117>
2. L. K. Pan, L. M. Chen, H. B. Zhang, C. Xu, C. Z. Yang, T. Xing, Research on vibration fatigue test method and device of integrated dropper, *Electr. Railway*, **31** (2020), 73–76. <https://doi.org/10.19587/j.cnki.1007-936x.2020z2.017>
3. P. H. Peng, L. M. Chen, W. Wang, F. He, The effect of frequency and amplitude of dropper on its fatigue life, *J. Railway Sci. Eng.*, **16** (2019), 471–477. <https://doi.org/10.19713/j.cnki.43-1423/u.2019.02.025>
4. X. Li, W. Z. Liu, C. Sun, J. H. Yi, M. Xu, Study on current collection characteristics of catenary based on new type of dropper, *Railway Stand. Design*, **65** (2021), 128–131. <https://doi.org/10.13238/j.issn.1004-2954.202001060004>

5. W. H. Zhang, G. M. Mei, X. J. Wu, L. Q. Chen, A study on dynamic behaviour of pantographs by using hybrid simulation method, *Proc. I. Mech. Eng. Part F*, **219** (2005), 189–199. <https://doi.org/10.1243/095440905X8880>
6. H. Zhao, X. H. Xiao, G. F. Qi, H. Y. Xu, H. M. Li, Analysis of fatigue life of catenary dropper for high-speed railway, *Eng. J. Wuhan Univ.*, **52** (2019), 351–357. <https://doi.org/10.14188/j.1671-8844.2019-04-011>
7. Q. Zhang, *Research on fatigue characteristics of catenary droppers of high-speed railway*, Shijiazhuang: Shijiazhuang Tiedao University, 2023. <https://doi.org/10.27334/d.cnki.gstdy.2022.000442>
8. D. F. Chen, *Analysis on the operation characteristics of the integral dropper of high-speed rail catenary and discussion on countermeasures*, Beijing: China Academy of Railway Sciences, 2020. <https://doi.org/10.27369/d.cnki.gtdky.2020.000049>
9. L. M. Chen, J. Sun, L. K. Pan, F. He, Analysis of dropper stress in a catenary system for a high-speed railway, *Math. Probl. Eng.*, **2022** (2022), 1–7. <https://doi.org/10.1155/2022/9663767>
10. F. He, D. D. Guo, The effects of load location on dropper stress in a catenary system for a high-speed railway, *Math. Probl. Eng.*, **2020** (2020), 1–10. <https://doi.org/10.1155/2020/7986141>
11. L. M. Chen, P. H. Peng, F. He, Fatigue life analysis of dropper used in pantograph-catenary system of high-speed railway, *Adv. Mech. Eng.*, **10** (2018), 1–10. <https://doi.org/10.1177/1687814018776135>
12. Y. Zhong, *A new approach to desired contact force between pantograph and overhead contact line system based on sliding electrical contact fundamental mechanism*, Cheng Du: Southwest Jiaotong University, 2020. <https://doi.org/10.27414/d.cnki.gxnju.2020.002536>
13. J. B. Guo, S. P. Yang, G. S. Gao, Study on active control of high-speed-train pantographs, *J. China Railway Soc.*, **26** (2004), 41–45. <https://doi.org/10.3321/j.issn:1001-8360.2004.04.009>
14. L. M. Chen, Study on dynamic force of integral dropper of catenary under action of high-speed pantograph, *China Railway Sci.*, **39** (2018), 86–92. <https://doi.org/10.3969/j.issn.1001-4632.2018.03.12>
15. S. G. Zhang, A finite difference method for second order ordinary differential equation of initial-value problem, *J. Chongqing Univ. Tech.*, **26** (2012), 110–112. <https://doi.org/10.3969/j.issn.1674-8425-B.2012.08.023>
16. A. G. Costello, *Theory of wire rope*, New York: Springer, 1997. <https://doi.org/10.1007/978-1-4612-1970-5>
17. Z. G. Yu, Z. R. Ge, Z. S. Niu, Z. Y. Zhu, Discussion on causes of failures and optimized schemes for OCS integrated droppers for high speed railway, *Electr. Railway*, **31** (2020), 10–14. <https://doi.org/10.19587/j.cnki.1007-936x.2020.01.003>
18. H. Li, M. Yazdi, *Advanced decision-making methods and applications in system safety and reliability problems*, Switzerland: Springer, 2022. <https://doi.org/10.1007/978-3-031-07430-1>

